Characterization of micropatterned nanofibrous scaffolds for neural network activity readout for high-throughput screening

Lina Wang, William S. Kisaalita

Cellular Bioengineering Laboratory, Faculty of Engineering, The University of Georgia, Athens, Georgia 30602

Received 31 October 2009; revised 10 February 2010; accepted 1 March 2010
Published online 12 May 2010 in Wiley InterScience (www.interscience.wiley.com). DOI: 10.1002/jbm.b.31646

Abstract: Micropatterns were fabricated in nanofibrous poly-L-lactic acid (PLLA) films by laser micromachining and the resulting scaffolds were characterized with respect to architecture, thermal, mechanical, and mass transport properties. Also, human neural stem cells were successfully cultured in these micropatterned nanofibrous scaffolds (MNFSs). The scaffolds were incorporated in high-density well plates (e.g., 96-well plates), creating a platform for high-throughput screening of drugs with physiologically more relevant networked neural cultures. Through mathematical modeling of the transport of model stimulants, the feasibility of stimulating neural networks cultured in MNFSs was demonstrated. More work is needed to establish biological network activity–MNFS architecture relationships. J Biomed Mater Res Part B: Appl Biomater 94B:238–249, 2010.

Key Words: nanofibrous PLLA scaffolds, laser micromachining, micropatterns, human neural stem cells, chemical depolarization

INTRODUCTION

Mental and/or neurodegenerative disorders, such as schizophrenia and Alzheimer's disease (AD), are among the most devastating illnesses in the western society. However, there are few effective drugs for such diseases[1]; for example, currently used drugs for schizophrenia still have shortcomings.[2] Drug discovery against these disorders is in great demand, which calls for effective screening of available molecular libraries to identify effective small molecules as drug leads. To quickly identify hits from diverse molecular libraries, cell-based assays together with automated high-throughput screening (HTS) are the state of the art.

Many studies have suggested that synaptic pathology and neurotransmission dysfunction underlies these biological mechanisms for mental and neurodegenerative disorders.[3] Neural networks, which can recapitulate these crucial targets, may act as a platform for screening available molecule libraries in drug discovery. *In vitro* screening of drugs that affect neural network function *in vivo* is still primitive as current assays rely on single cellular responses from two-dimensional (2D) cell cultures. Three-dimensional (3D) cell-based assays may yield physiologically more relevant results and thus have the potential to bridge the gap between 2D assays and preclinical animal testing, saving time and cost by improving clinical efficacy predictability. Thus, engineering a platform for 3D neural network patterning *in vitro* for HTS system is an ideal first step to move to 3D neural network–based assay.

To pattern neural networks formation *in vitro*, chemical patterning and structural guiding[4,5] are commonly used methods. Microlithographic materials and techniques,[6] microcontact printing,[7,8] and self-assembled monolayers[9] are mainly used to tailor the properties of the substrates for patterning neural cell growth. However, these cells are maintained on 2D substrates. Topographical structures can provide physical guidance for neural network formation *in vitro* and micropatterned substrates have long been considered a promising approach for the creation of defined neuronal networks *in vitro*. High-aspect-ratio microstructures are thought to provide quasi-3D microenvironments with well-defined architectures for neural cell growth and neural network formation.[10,11] Microstructures made of polydimethylsiloxane (PMDS)[12] and SU-8 (epoxy-based negative photoresist)[13] have been reported to control neuronal outgrowth and synapse formation *in vitro*. However, these structures are devoid of natural extracellular matrix (ECM) architecture with respect to nanofibrous structures.

To best mimic the architecture of the natural ECM, nanofibrous scaffolds have been fabricated using phase separation,[14] electrospinning,[15] and self-assembly.[16] The nanofibrous scaffolds are able to promote the differentiation of neural stem cells[17,18] and induce "3D matrix adhesion" as defined by Cukierman et al.[19] in human fibroblast cells. These nanofibrous structures have been combined with microporous structures for tissue engineering.[20] In this study, we aimed to combine the effects of nanofibrous scaffolds on neural stem cell differentiation and that of microstructures on neural network patterning, to provide micropatterned nanofibrous scaffolds (MNFSs) for neural network

Additional Supporting Information may be found in the online version of this article.
Correspondence to: W. S. Kisaalita; e-mail: williamk@engr.uga.edu
Contract grant sponsor: NSF; contract grant number: ECS-0304340.
Contract grant sponsor: UGA

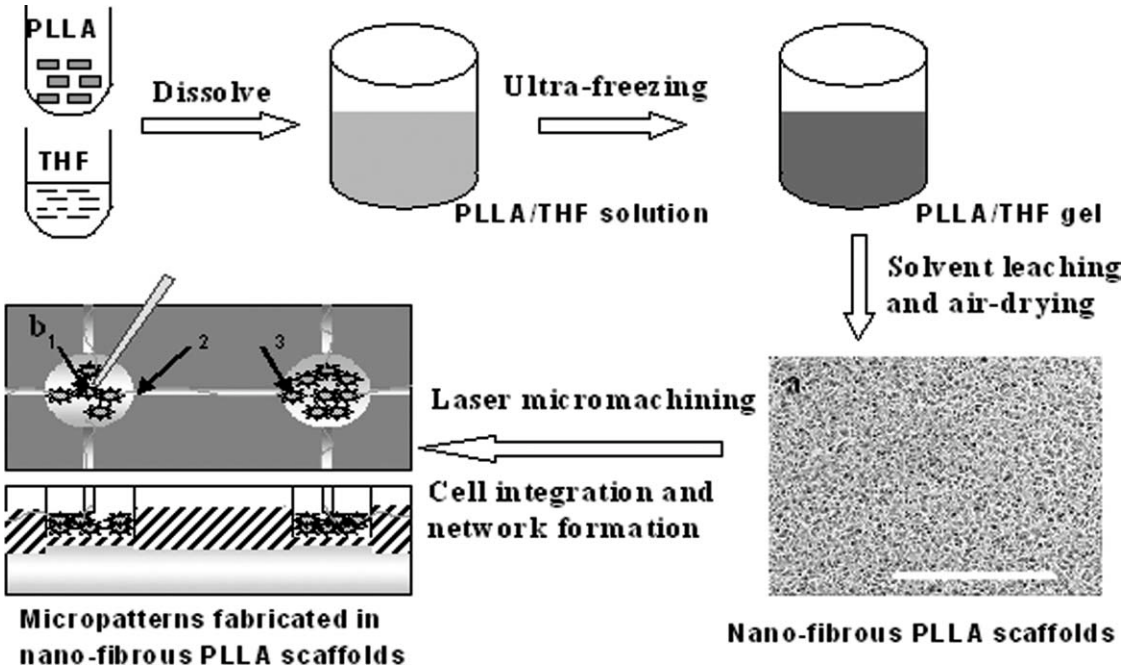

FIGURE 1. Flow diagram of the fabrication process: (a) the resultant nanofibrous PLLA structure; (b) the schematic of micropatterns fabricated in nanofibrous PLLA film; the top is the top view and the bottom is the cross-section view. Assuming a neural network in the microstructure unit, stimulus would be added through a micropipette to the cell at the center of the stimulus microwell (postion 1). Cellular signal (e.g., calcium wave) would propagate from the stimulus microwell (position 1) to the neighboring well (position 3) within this neural network; meanwhile, the stimulating compound would diffuse from the stimulus well (position 1) to the neighboring well (position 3). Scale bar = 100 μm.

formation *in vitro*. Furthermore, we aimed to integrate the MNFSs with currently used HTS systems (e.g. 96-well plates) for neural network activity readout.

To study neural network activity, depolarizing neural cells by chemicals and observing signal propagation (such as calcium wave propagation stimulated by high concentration potassium buffer) is one commonly used method.[21] With the development of fluorescence-based technologies and their implementation in HTS systems, for example, fluorometric imaging plate reader (FLIPR), neural network–based assay combined with fluorescence imaging could be an invaluable tool in drug discovery, especially for screening drugs or compounds against neural network activity. In such an application, one main concern is to distinguish whether the signal propagation observed in the network is due to cell-to-cell connectivity or due to stimulant compound diffusion from the injection spot. Thus, the third aim was to simulate model stimulant compound transport to compare chemical diffusion to signal propagation in MNFSs with the goal of establishing the feasibility of stimulating neural networks by chemical means in this platform.

MATERIALS AND METHODS

Fabrication of nanofibrous scaffold

The nanofibrous scaffold was fabricated by the liquid–liquid phase separation method using poly-L-lactic acid (PLLA).[14] Figure 1 shows the flow diagram for the fabrication process. Briefly, PLLA (Sigma, St. Louis, MO), was homogeneously dissolved in tetrahydrofuran (THF) at various concentrations (1.25–5% wt/v). On the basis of previous studies[14] and a preliminary study in our group (data not shown), it was found that when the PLLA in THF concentration increased (such as 9% wt/v), the resulting solution became very viscous and the fabricated scaffold lacked the porous and nanofibrous architecture. When the concentration was too low (such as 1% wt/v), the formed gel was very fluffy and unstable in cold water. Thus the range 1.25–5% wt/v was chosen in this study. Four milliliters of the PLLA/THF solution was prewarmed at 55°C and then quickly cast onto a glass Petri dish (8 cm in diameter) followed by ultra-freezing at −80°C for 2 h. The gelled PLLA/THF solution was immersed into cold double distilled water (4°C) for 2 days to leach out the solvent (THF). Water was changed three times every day and the resultant PLLA structure was air dried. PLLA scaffolds without nanofibrous structures were fabricated following the same procedure but without the ultra-freezing process.

Characterization of nanofibrous PLLA scaffolds

Scanning electron microscope observation. PLLA scaffolds were sputter-coated with gold for 60 s to achieve a coating thickness of about 15.3 nm. SEM images were captured with a FEI Inspect-F scanning electron microscope (SEM) (FEI Company, OR). Fiber diameters were measured with Simple PCI image software (Compix, Cranberry Township, PA).

Porosity measurement. The porosity values of the nanofibrous scaffold were measured by liquid displacement.[22] Ethanol was used in our procedure because it penetrated

easily into the pores and did not induce shrinkage or swelling. Student's *t*-test was used for statistical comparisons of fiber diameter and porosity.

Diffusivity measurement by fluorescence recovery after photobleaching (FRAP). Diffusion coefficients of both small and large molecular weight compounds were measured with fluorescein sodium and FITC-dextran. Fluorescein sodium, USP (MW = 332, Allied Chemical, India) was chosen because it is similar in size to many small molecular weight drugs, such as ketamine (MW = 238). FITC-dextran (~40 kDa, Sigma-Aldrich) was selected because it is similar in size to some large molecular weight compounds in media, such as leukemia inhibitory factor (LIF, ~32–62 kDa).

All FRAP experiments were performed on a Leica DMI 6000B microscope with Leica TCS SP5 LAS AF FRAP wizard (Leica Application Suite Advanced Fluorescence). Samples were incubated with fluorescein sodium (30 μM) or FITC-dextran (30 μM) at 4°C overnight. Before testing, samples were equilibrated at room temperature for 30 min, and all tests were performed at room temperature (25°C). FRAP experiments were carried out in the middle of the scaffolds. The middle zone FRAP experiments were performed at approximately half of the scaffold thickness from the surface. All photobleaching were performed with an argon laser at 100% power (100 mV, 488 nm emission) for 394.5 s. Images in recovery process were performed with an argon laser at 5% power for 395.4 s (300 frames, with an interval of 1.315 s). All images were recorded with a 20×/0.5 HCX PL APO CS 0.70 DRY UV objective (Leica). Images were 512 by 512 pixels.

Diffusion coefficients were calculated from the FRAP experiments using the method described by Axelrod et al.[23] Briefly, the mean fluorescence in the bleached region over time was converted to a normalized fractional fluorescence intensity

$$f = F(t) - F(0)/F(\infty) - F(0) \quad (1)$$

where $F(t)$ is the fluorescence intensity at time t, $F(0)$ is the fluorescence intensity immediately after bleaching, and $F(\infty)$ is the fluorescence after complete recovery. The fractional fluorescence intensity was plotted versus time and fitted with a logarithmic curve. The recovery rate varied with size of the bleached area, location of the bleached area, and the size of the diffusing molecule.[24] The equation for the curve was used to determine the half-recovery time ($\tau_{1/2}$) at $f = 0.5$. The bleaching parameter, which describes the relationship between the half-recovery time and the characteristic diffusion time, was also calculated according to Axelrod et al.[23] The half-recovery time, $\tau_{1/2}$, the measured initial spot radius ω, and the bleaching parameter, γ_D,[23] were used to determine the diffusion coefficient, D:

$$D = (\omega^2/4\tau_{1/2})\gamma_D \quad (2)$$

Thermal properties. The thermal properties of air-dried PLLA scaffolds were characterized by differential scanning calorimetry (DSC). The Thermal Analysis Instruments Mettler Toledo DSC 823[e] (Mettler-Toledo, Columbus, OH) was operated in standard mode using an aluminum pan reference with a nitrogen purge rate of 50.0 mL/min. The standard mode DSC heating program was equilibrated at 20°C and the ramp temperature set at 10°C /min to 200°C. Glass transition temperature (T_g), the melting temperature (T_m), and the enthalpy of melting of PLLA (ΔH_m) were determined. The degree of crystallinity (X_c) was calculated as $X_c = \Delta H_m/\Delta H_m^0$, where ΔH_m^0 is the enthalpy of melting of 100% crystalline PLLA. The calculated value of ΔH_m^0 is 93.7 J/g.[14,22]

Mechanical property. The compressive modulus of the nanofibrous PLLA scaffolds (5% wt/v) was measured at ambient temperature. The samples were tested on an Instron Model 3344 Materials Testing Machine (Instron Co., Canton, MA). Scaffolds were cut into pieces (~10 mm in length and 10 mm in width) for testing. Samples were compressed at a displacement rate of 0.6 mm/min. Four different samples were tested and only 5% (wt/v) samples were tested because lower concentration samples were too weak for this test.

Optical property of micropatterns. Light transmittance of polymer scaffolds at the pattern position was measured by a microscope (BX40, Olympus) coupled with a digital camera (D100, Nikon). Images were taken with the same lamp power and exposure time. These images were processed with SimplePCI 2000 software. The light transmittance ratio was calculated by dividing the sample mean grey level from three different spots by the control gray level (plain cover slips).

Surface energy and contact angle measurement. Contact Angle System OCA (Future Digital Scientific Corp.) with analysis software (SCA20) was used to determine the surface contact angles on the nanofibrous PLLA samples both before and after NaOH treatment. Distilled water was used as a contacting solvent. All data were obtained 5 s after placing the droplet on the surfaces under ambient conditions. The surface energy of the contacting surface (E_s) was calculated according to $E_s = E_{lv}\cos\theta$. E_{lv} is the surface energy between the water and air, which is 72.8 mJ/m^2 at 20°C for pure water; θ is the static contact angle.[25]

Fabrication of MNFSs

Nanofibrous PLLA scaffolds were micromachined with a computer-controlled laser system composed of a workstation (Rapid X250 from Resonetics, NH), an excimer laser (ATLEX 500SI from ATL, Wermelskirchen, Germany) coupled to argon fluoride (RrF, 193 nm wavelength) gas (Spectra Gases, NJ). The direct write approach was used as micromachining mode. Using appropriate mask sizes, channels (10–20 μm wide) and wells (up to 100 μm in diameter) were fabricated into the nanofibrous structure, creating high-aspect-ratio MNFSs.

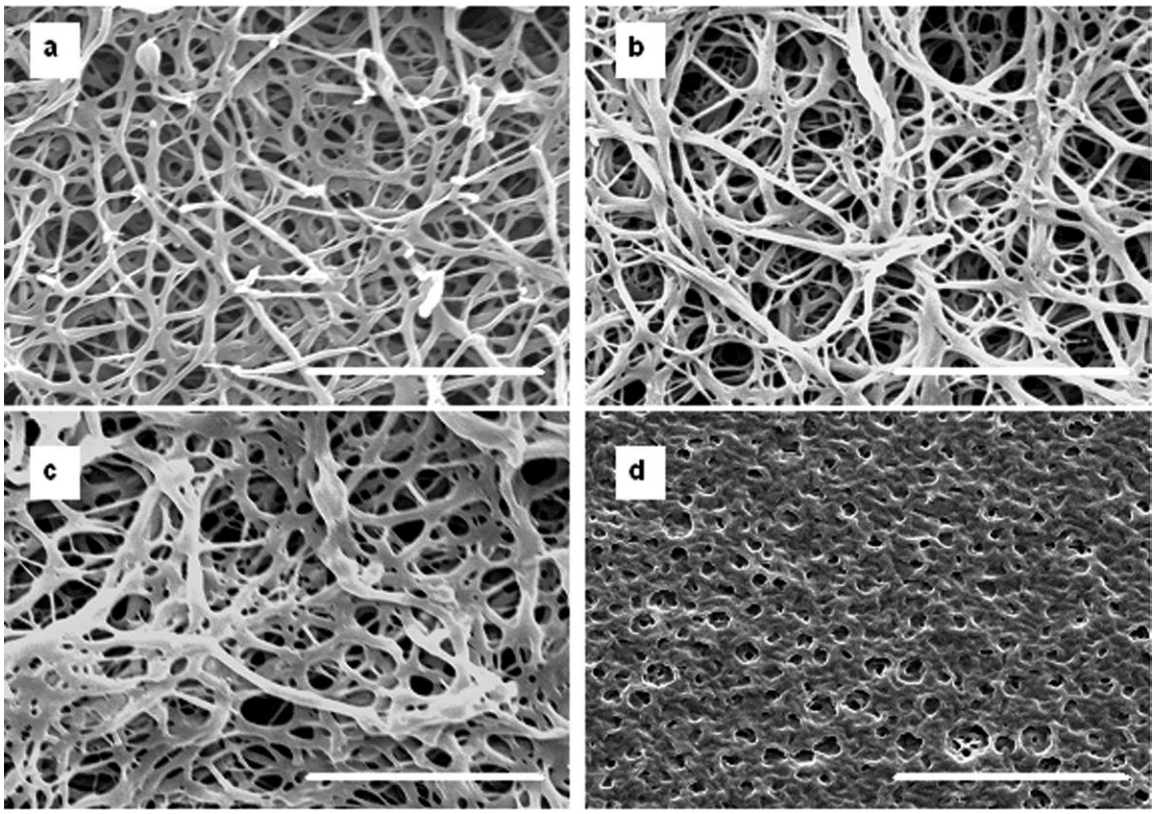

FIGURE 2. SEM images of nanofibrous PLLA scaffolds prepared at different concentrations of PLLA in THF (a–c): (a) 1.25% wt/v; (b) 2.85% wt/v; and (c) 5% wt/v. (d) shows 5% wt/v PLLA in THF scaffolds without nanofibrous structures. Scale bar = 5 μm in (a–c) and 20 μm in (d).

Integration of MNFSs with 96-well plates

MNFSs were cut into pieces that can fit into the wells of 96-well plates (*In Vitro* Scientific, Sunnyvale, CA) using laser micromachining with the Rapid X 250 Excimer System (Resonetics, Nashua, NH). Then PLLA pieces were glued on the bottom of these wells by MONO AQUA liquid glue that is transparent and nontoxic (American Tombow, Suwanee, GA).

Simulation of chemical diffusion in MNFSs

As depicted in Figure 1(b), a stimulating compound was added through a micropipette to an imaginary cell at the center of the stimulus microwell (i.e., postion 1). If the stimulus concentration at position 1 reached the threshold value (e.g. voltage-gated calcium channel opening), cellular response at position 1 and signal propagation (e.g. calcium wave propagation) from the stimulus microwell (position 1) to the neighboring wells (i.e., position 3) would be induced. Meanwhile, the stimulating compound would diffuse from position 1 to position 3. At the time it took the signal to reach cells at position 3, the stimulus concentration due to diffusion was compared with the threshold value for inducing cellular response; confirming that the cellular response that would be observed at position 3 would only be due to network connectivity and not the diffusing chemical.

Diffusion of small molecular weight compounds within MNFSs was simulated with COMSOL Multiphysics 3.5a (COMSOL, MA). Fluorescein was chosen to represent small molecular weight compounds. Fluorescein (500 mM[11]) was added through a micropipette with a tip opening of 6, 20, or 50 μm. And the threshold value for stimulating cell response was assumed to be 50 mM.[11] Diffusivity of fluorescein in water is 640×10^{-12} m^2/s[26] and that of fluorescein in nanofibrous PLLA scaffolds (5%) was measured as described above. Calcium waves have been observed to travel at a speed ranging from 10 to 100 μm/s.[27] A calcium wave propagating speed of 43 μm/s[21] was assumed. Microwell diameter was 50 μm and channel width was 10 μm; two channel lengths (70 and 100 μm) were investigated.

Cell line and cell culture

Human neural stem cells ENStem-A™ were purchased from Millipore (Billerica, MA) and maintained in 35 mm Petri dishes with 2 mL growth medium in a 5% CO_2 humidified atmosphere at 37°C. ENStem-A™ expansion media supplemented with penicillin/streptomycin, L-glutamine and basic fibroblast growth factor (bFGF). The medium was changed every other day. The cells were passaged by mechanically pipetting when progenitor cells reached 90–100% confluence, around 1.2×10^6 cells were seeded into each new dish. Prepared nanofibrous PLLA micropatterns were treated with 0.2M NaOH for 40 min at 40°C to increase the surface hydrophility. Then samples were sterilized by immersion in 70% ethanol in distilled water (DI) under a

TABLE I. Fiber Size Distribution of Nanofibrous Scaffolds Fabricated With Various PLLA Concentrations

Concentrations of PLLA in THF Solution (% wt/v)	1.25	2.85	5
Fiber diameter (mean ± SD) (nm)	202.8 ± 33.9 ($n = 77$)	238.2 ± 45.1[a] ($n = 49$)	293.6 ± 49.4[a,b] ($n = 38$)
Porosity (%)	92.2 ± 3.0 ($n = 3$)	85.9 ± 0.2[a] ($n = 3$)	84.9 ± 1.2[a] ($n = 3$)

[a] $p < 0.05$. Compared with the data of 1.25% (wt/v) PLLA scaffold.
[b] $p < 0.05$. Compared with the data of 2.85%(wt/v) PLLA scaffold.

UV germicidal lamp overnight. After sterilization, they were rinsed in sterile DI water three times. The substrates were then coated with polyornithine (Sigma, St. Louis, MO) in water at a concentration of 40 μg/mL for at least 1 h. This was followed by coating with laminin (Sigma, St. Louis, MO) at a concentration of 5 μg/mL. These dishes were stored at 4°C unstill use.

Fluorescence staining and fluorescent microscopy

Neural stem cells were stained with calcein AM (Biotium, Hayward, CA). This fluorescent dye stains live cells and their extensions by the presence of intracellular esterase activity, which converts the nonfluorescent cell-permeant calcein AM to intensely fluorescent calcein. Cells were washed with 2 mL Neurobasal without phenol red (Invitrogen, Carlsbad, CA) three to five times. Then cells were exposed to 2 mL of 2 μ*M* calcein AM in neurobasal and incubated for 30 min at 37°C before the staining solution was replaced. Samples were washed with neurobasal three times. Sample fluorescence was viewed and captured with a B-2E/C FITC filter block (Nikon, Melville, NY), which has an excitation bandwidth of 465–495 nm and a filter pass range of 515–555 nm.

SEM observation

Cells on PLLA patterns were fixed with 2% glutaraldehyde in 0.1*M* sodium cacodylate buffer (pH 7.2) for 1 h and then rinsed in cacodylate buffer three times (15 min each). This was followed by postfixing with 1% OsO_4 in 0.1*M* sodium cacodylate buffer for 1 h and rinsing in cacodylate buffer three times (5 min each). The samples were then dehydrated in 35, 50, 70, 80, 95, and 100% ethanol successively for 10 min each and dried in Hexamethyldisilazane (HMDS, Sigma, St. Louis, MO). Scaffolds were sputter-coated with gold for 60 s to achieve a thickness of about 15.3 nm. SEM images were captured with a FEI Inspect-F SEM (FEI Company, OR).

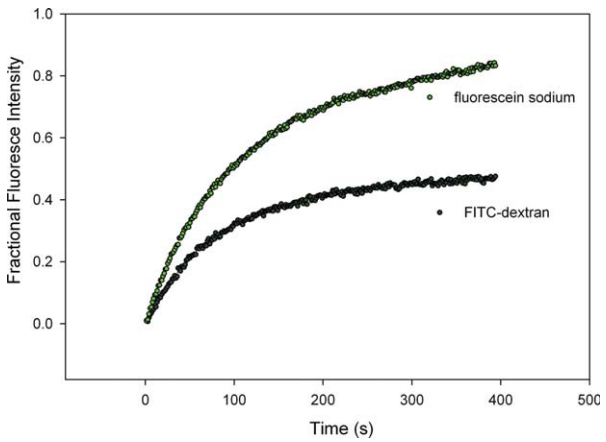

FIGURE 3. Examples of fluorescence intensity recovery in the bleached region versus time after bleaching in 2.85% (wt/v) PLLA in THF scaffolds. [Color figure can be viewed in the online issue, which is available at www.interscience.wiley.com.]

RESULTS AND DISCUSSIONS

Characterization of nanofibrous PLLA scaffold

Structure, porosity, and mass transfer within scaffolds. - Figure 2 shows the SEM images of nanofibrous PLLA scaffolds prepared at different concentrations of PLLA in THF. Fiber diameters were measured and the results are presented in Table I. It was found that the fiber diameters increased significantly ($p < 0.05$) when the PLLA concentration increased. These fibers were all at submicro scale (~200–300 nm), which is close to the size range of collagen matrix (~50–200 nm). Thus the nanofibrous structures could mimic the architecture of the natural extracellular matrix (ECM) with respect to fiber size.

The nanofibrous PLLA scaffolds were highly porous as shown in Table I. Compared with PLLA scaffolds without nanofibrous structures which had a porosity of 53.85%, the porosities of nanofibrous PLLA scaffolds were above 80%. As the PLLA concentration increased, the scaffold porosity decreased (Table I). However, the porosity was still above 80%. These results were consistent with results for freeze-dried PLLA nanofibrous scaffolds,[14] suggesting that the drying method may not be a factor in resultant porosity.

Highly porous PLLA scaffolds allowed molecular diffusion within the scaffolds, ensuring cells in the scaffolds enough exposure to chemicals in the media. In cell culture media, compounds vary from small molecules (MW < 1 kDa) to large ones (MW ~ 60 kDa). And fluorescein sodium and FITC-dextran were selected to represent these compounds. Diffusivities of fluorescein sodim and FITC-dextran in PLLA scaffolds with different PLLA concentrations in THF (2.85 and 5%) were studied by FRAP. Figure 3 presents examples of fluorescence intensity recovery in the bleached region vs. time in 2.85% (wt/v) PLLA scaffolds. As expected, larger molecules diffused much slower than small

TABLE II. Thermal Properties of PLLA Nanofibrous Scaffolds Determined by DSC

Concentrations of PLLA/THF Solution (% wt/v)	T_g (°C)	T_m (°C)	X_c (%)
1.25	67.62	175.39	56.64
2.85	64.88	176.65	56.98
5	64.14	175.74	56.52

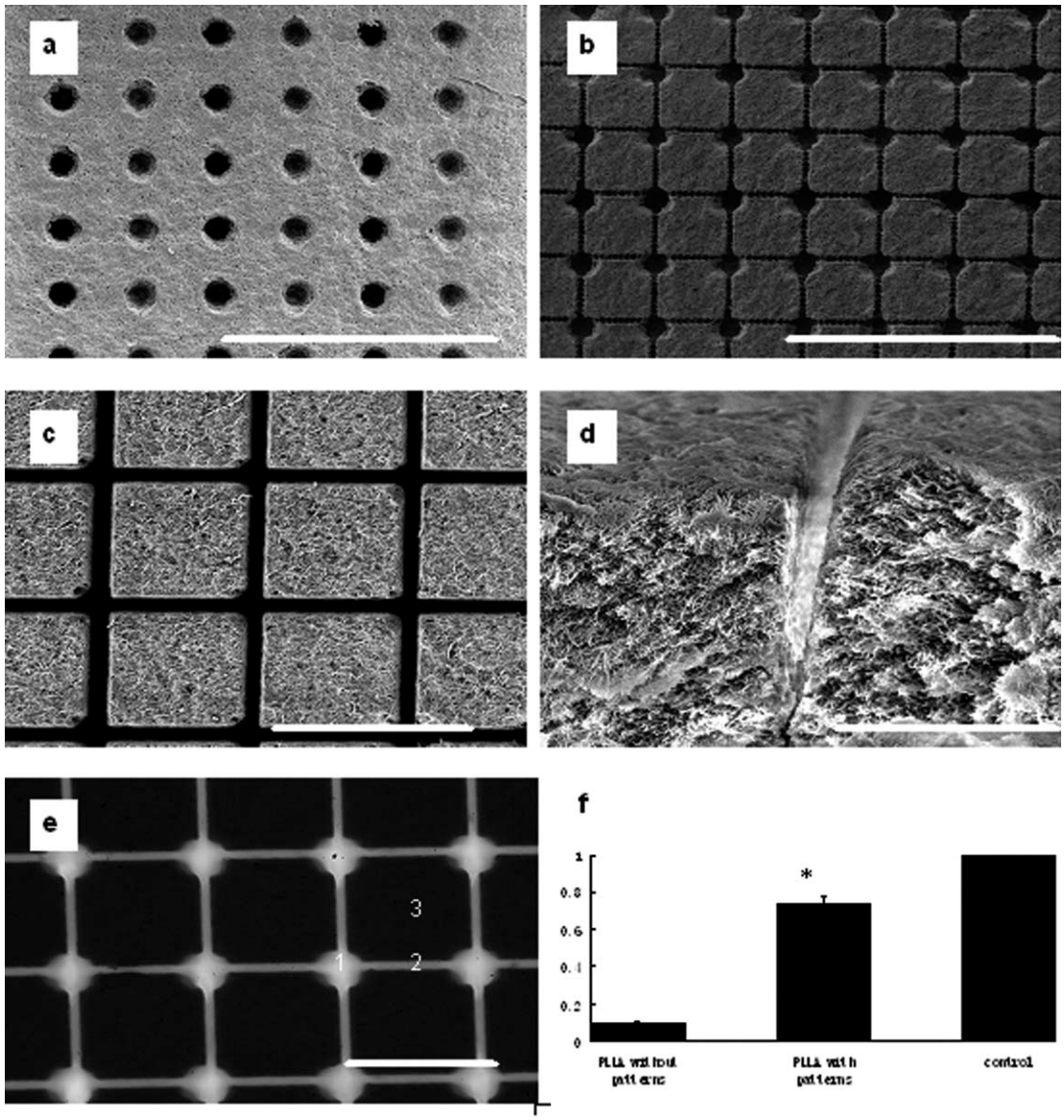

FIGURE 4. SEM images (a–d) of micropatterns fabricated in nanofibrous PLLA in THF scaffolds (5% wt/v). (a) A microwell array. (b) A network pattern consisting of microwells and channels. (c) A network pattern consisting of channels only, without microwells. (d) The crosssection of a channel in the scaffold. (e) Phase contrast image of micropatterned nanofibrous scaffolds (MNFSs) as in (b). (f) The light transmittance profile at the positions with micropatterns (such as position 1 and 2 in (e)) and without micropatterns (such as position 3 in (e)); * indicated that the light transmittance ratio at the position with patterns was significantly higher than that at the position without patterns. Scale bar = 500 μm in (a) and (b), 200 μm in (c) and (e), and 50 μm in (d).

molecules. In 2.85% (wt/v) PLLA scaffolds, diffusivity of fluorescent sodium was 124.38 ± 2.02 $\mu m^2/s$ ($n = 3$) and diffusivity of FITC-dextran was 5.26 ± 0.28 $\mu m^2/s$ ($n = 3$); in 5% (wt/v) PLLA scaffolds, diffusivity of fluorescent sodium was 104.31 ± 1.90 $\mu m^2/s$ ($n = 3$) and diffusivity of FITC-dextran was 4.21 ± 0.50 $\mu m^2/s$ ($n = 3$). The measured diffusion coefficient of fluorescein sodium in 5% PLLA is smaller than that in water.[26,28]

Mechanical property and thermal property. As supportive substrates for cell culture and platforms for HTS application, sufficient mechanical strength of the scaffolds is required. The compressive modulus of the nanofibrous PLLA scaffolds (5% wt/v) was measured. The nanofibrous PLLA scaffolds had a compressive modulus of 9.65 ± 0.43 MPa ($n = 4$). Compared with the modulus of freezing-dried nanomicro-PLLA scaffolds which was within 50 kPa,[29] the increase in film stiffness may be due to the air-drying process. Mechanical cues from microenvironments, such as substrate modulus, affect cell behavior, especially directing neural stem cell differentiation.[30,31] According to these studies, neural tissues preferred substrates with a modulus of the brain tissue (around 500 Pa). In our case, the nanofibrous PLLA substrates are too stiff to provide an in-vivo like substrate for neural cell growth with respect to stiffness. However, the architecture of microwell structures promoted cellular

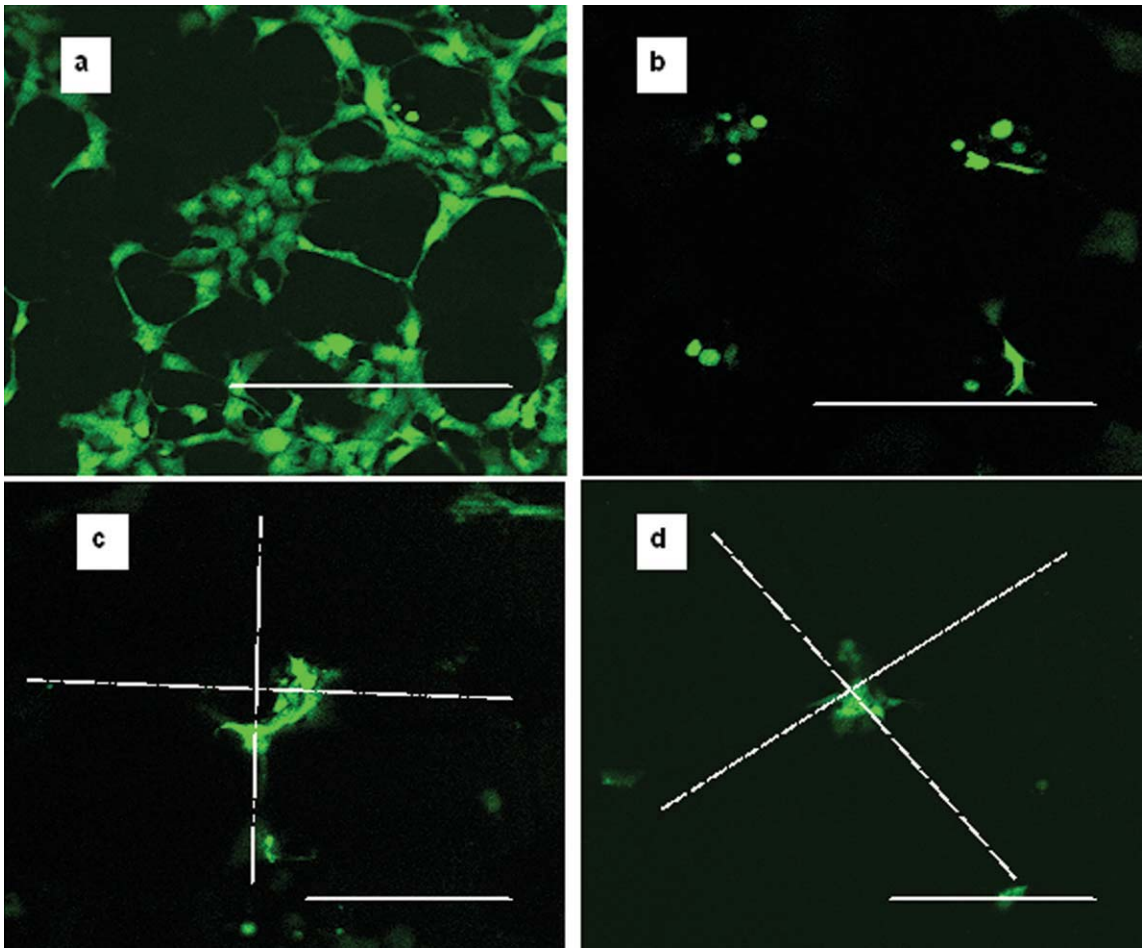

FIGURE 5. Fluorescence images of calcein stained neural stem cells: (a) on 2D nanofibrous PLLA substrate. (b–d) Within MNFSs; the network pattern used consisted of microwells (100 μm in diameter and 50 μm in depth) and channels (10 μm wide) with general architecture shown in Figure 4(e). (c, d): cells attached to the sidewalls of microwells or formed clusters in the wells; dotted line shows the position of channels. Scale bar = 150 μm in (a) and (b), 100 μm in (c) and (d). [Color figure can be viewed in the online issue, which is available at www.interscience.wiley.com.]

cluster formation within the microwells (as shown in Figures 5 and 6). Cell–cell contact within the clusters could become dominant for cell differentiation. Thus, the nanofibrous PLLA micropatterns are still promising in providing a microenvironment which favors neural stem cell growth and differentiation.

Though PLLA has gained much interest in tissue engineering, its lower melting temperature and lower ability of crystallization limit its widespread application.[32] Thermal properties were studies by DSC and the results are presented in Table II. The average glass transition temperature (T_g) and the average melting temperature (T_m) of nanofibrous PLLA scaffolds were 65.55 and 175.93°C, respectively. The average crystallinity (X_c) was found to be 56.71%. PLLA scaffolds without nanofibrous structures (5% wt/v) were fabricated without ultra-freezing process and their thermal properties were characterized by DSC. These PLLA scaffolds without nanofibrous structures (5% wt/v) had a lower T_g (53.46°C) and a lower X_c (31.11%) than nanofibrous PLLA scaffolds (5% wt/v), indicating that the thermal properties and crystallization properties have been improved in nanofibrous PLLA scaffolds.[32] Thus, the nanofibrous PLLA scaffolds have great potential as high performance polymers for HTS systems.

Fabrication and characterization of MNFSs

Laser micromachining is a powerful tool for microstructure fabrication. It is capable of cutting, drilling, etching, stripping, and skiving materials such as polymers, plastics, glass, semiconductor materials, ceramic, and thin metals. And achievable microstructure dimension ranges from 1 μm to 1 mm. Figure 4 shows different micropatterns fabricated in nanofibrous PLLA films. The "direct write" approach was used as the micromachining mode. Using appropriate mask sizes, channels (around 10 μm) and wells (up to 100 μm) were fabricated into the nanofibrous structure. The depths can be controlled by the number of laser pulses (data not shown) or energy level (which was kept constant in this study). Laser micromachining can be directly applied to different kinds of polymers using direct write approach, which provides flexibility in material choices, fabrication techniques, and pattern design. In addition, the fabrication

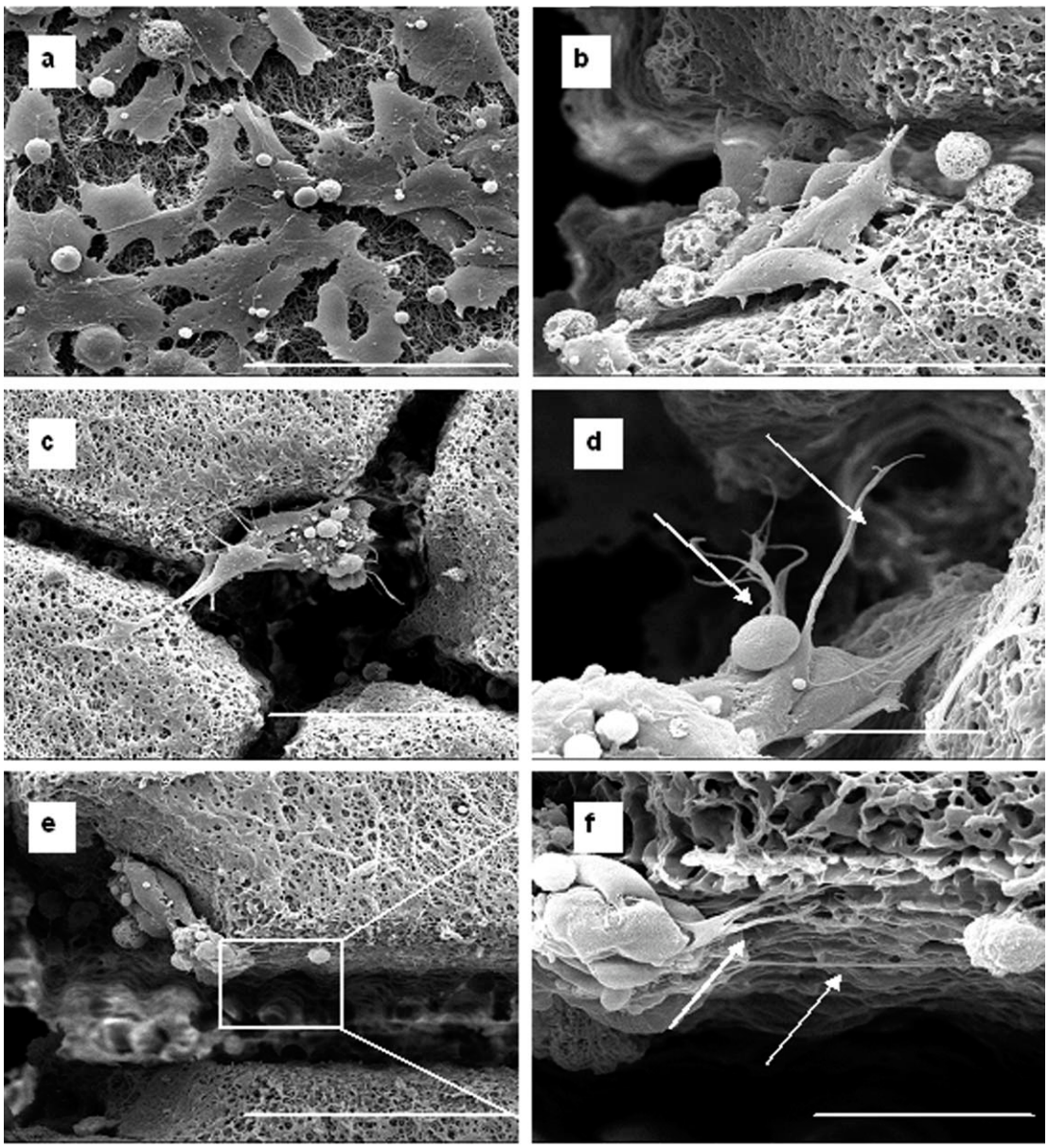

FIGURE 6. SEM images of neural stem cells: (a) on 2D nanofibrous PLLA substrate. (b–f) In a network pattern consisting of microwells and channels [as in Figure 4(e)]. (b, c) Attached to the sidewalls of microwells or formed clusters in the wells. (d–f) Neurite extensions observed in the well and along the channel (arrows). Scale bar = 50 μm in (a), (c) and (e), 30 μm in (b), and 10 μm in (d) and (f).

technique avoids use of chemical reagents that may introduce undesirable effects for cell culture applications. Furthermore, using this technique, it is possible to produce microstructured units in sufficiency to meet the need in HTS.

Compared with the microstructures derived through traditional microfabrication using SU-8 or PDMS, micropatterns based on nanofibrous PLLA scaffolds have high porosity (as shown in Section Structure, porosity and mass transfer within scaffolds). Also, nanofibrous structures provide extra cellular matrix contact for cell attachment that mimics *in vivo* extracellular collagen fibers in terms of scale. However, PLLA scaffolds are opaque, which is unfavorable for optical detection methods. To solve this problem, microwells in PLLA scaffolds were drilled through, leaving a thin film at the bottom and making cells in the wells optically accessible [Figure 1(b)]. Figure 4(e) shows a phase contrast image of the MNFSs in Figure 4(b). From Figure 4(f), it is evident that the light transmittance at the positions with microstructures was improved.

Prepared MNFSs were hydrophobic, which is unfavorable for cell culture. To tailor the surface property for cell culture purpose without changing nanofibrous structures, MNFSs were treated with 0.2*M* NaOH. Studies have shown that NaOH treatment on PLLA increased material wettability and surface roughness at nanometer scale.[33] Modification of

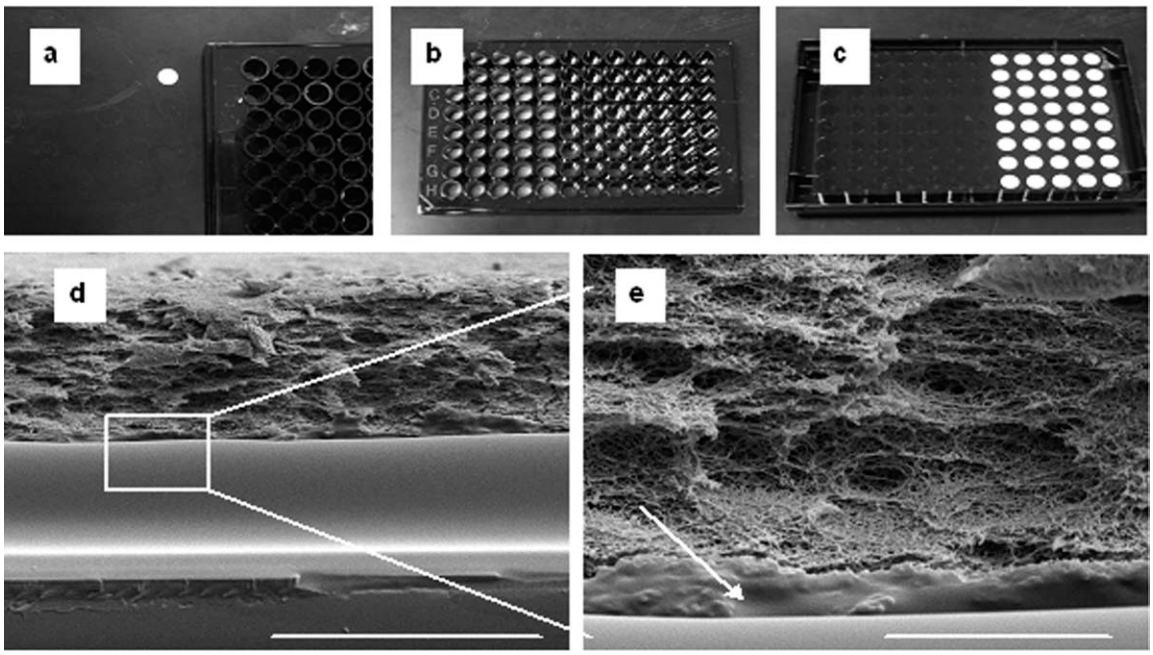

FIGURE 7. (a) A small round piece of MNFSs which was cut by laser micromachining according to the dimension of 96-well plates; (b, c) the top (b) and bottom (c) views of 96-well plates after integration of MNFSs. (d, e) SEM images of nanofibrous PLLA scaffolds glued onto the plate glass bottom. At the interface of PLLA scaffold and glue, the nanofibrous structures were sealed by glue (arrow); but most of the PLLA film still kept the nanofibrous structures as shown in (d) and (e). Scale bar = 100 μm in (d) and 20 μm in (e).

surface wettability/energy can be used to improve cell adhesion and proliferation.[25,33] Through base hydrolysis treatment, the contact angle of PLLA film decreased from 116.4° to 46.4°, and surface energy increased from −32.3 to 50.2 mJ/m^2. The modified PLLA surface would be suitable for cell attachment. Figures 5 and 6 show cell integration with MNFSs. Cell patterning in a network pattern consisting of microwells and channels [as in Figure 4(e)] can be observed in Figure 5(b). Cells attached to the inside walls of the microwells and formed clusters within the wells [Figure 5(c,d)]. Neurite extension was also observed along the microchannels [Figure 5(c)]. These observeations were confirmed by SEM images in Figure 6. Thus, we successfully integrated neural stem cells with MNFSs. The nanofibrous PLLA based micropatterns can provide physical guidance for neural network formation *in vitro*.

Integration of MNFSs into high-density well plates

To demonstrate potential for MNFSs in HTS system, MNFSs were integrated with 96-well plates. These films were cut into pieces that fit 96-well plate [Figure 7(a)]. The pieces were then glued on the bottom of these wells with a nontoxic glue [Figure 7(b,c)], which did not affect the nanofibrous structures of PLLA scaffolds [Figure 7(d)]. The glue formed a thin film between PLLA scaffold and glass [Figure 7(d)]. The glue sealed the nanofibrous structures only at the interface of glue film and PLLA scaffolds [Figure 7(e)]. The glue is transparent and the thin glue film did not block light transmission (data not shown). Combined with fluidic handing, this process can be adapted to any other currently used cell culture dishes or plates (24-well, 384-well plates), providing ready-to-use convenience and automated instrumentation compatibility. Our future study will characterize neural stem cell differentiation and network connectivity within nanofibrous PLLA micropatterns, which will provide a proof-of-concept for network-based platform for biosensing in drug screening.

Simulation of chemical diffusion in MNFSs

Figure 8(a) presents the fluorecein concentration profiles at different positions in MNFSs after injecting from the tip. At position 1, the stimulus concentration drops abruptly from initial 500 m*M* to around 16 m*M* at 0.1 s. Thus, the concentration at position 1 reaches the threshold value of 50 m*M* within 0.1 s, and the cell at position 1 would get stimulated. At position 2, the concentration increases to about 4 m*M* and then decreases to 0 gradually, which is lower than the threshold value and could not induce cellular response. This indicates that 6 μm wide tip can be used to chemically stimulate single cell without affecting cells nearby. The concentration at position 3 increases slightly to a value above 0; and the process happens very slowly. A calcium wave propagation, traveling at 43 μm/s, takes around 3.5 s to reach the neighboring well from the stimulation spot when the channel length is 150 μm. At that time, the concentration at position 3 is still lower than the threshold value for inducing cellular response (Table III). Thus, if cellular response is observed at position 3, it would be caused by cell–cell interaction within the network rather than stimulus diffusion. Thus, using these MNFSs for studying neural network activity by chemical stimulation is feasible. Figure 8(b) shows

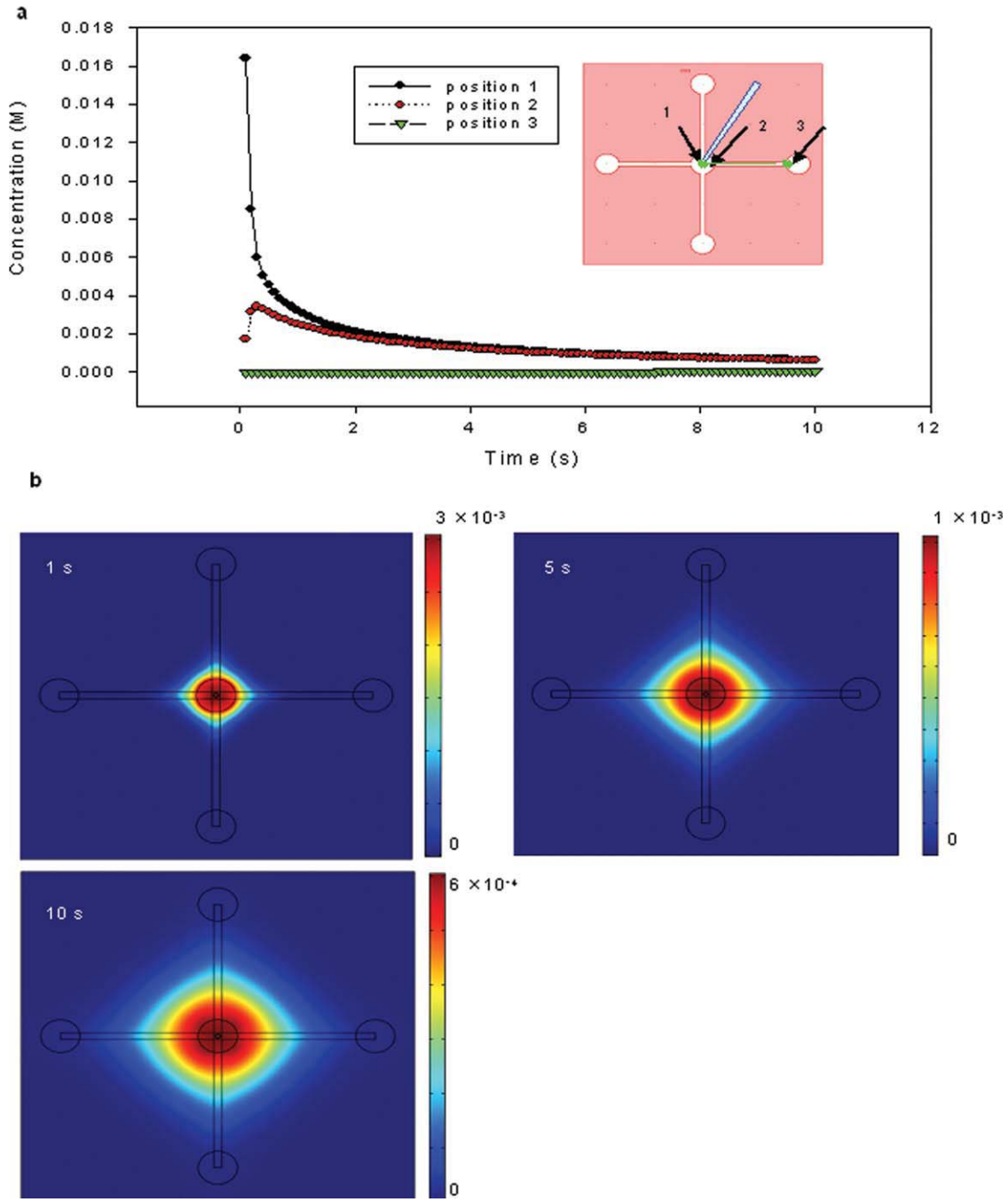

FIGURE 8. Simulation of fluorescein diffusion in MNFSs. (a) The micropatterns had microwells of 50 μm in diameter, with channel width and length of 10 and 150 μm, respectively. The diffusion of 500 m*M* fluorescein added through a micropipette with a tip diameter of 6 μm at postion 1 in the stimulus well was simulated (inset). Plots show fluorescein concentrantion profiles at positions 1, 2, and 3. (b) Simulated fluorescein diffusion in the MNFSs from the stimulus well to the neighboring well at 1, 5, and 10 s after fluorescein addition. [Color figure can be viewed in the online issue, which is available at www.interscience.wiley.com.]

TABLE III. Fluorescein Concentration (μ*M*) at the Opening of the Neighboring Microwell [Position 3 in Figure 8(a)] After Injection in the Stimulus Well [Position 1 in Figure 8(a)]

Channel Length	1 s	1.6 s	3.5 s	5 s	10 s
$L = 70$ μm	19.550187	**41.130028**	107.31041	140.20906	186.13265
$L = 150$ μm	0.016366172	0.1506446	**2.1177968**	4.931653	17.760927

Five hundred micromolar fluorescein was injected with a tip of 6 μm in diameter. Two channel lengths (70 and 150 μm) were used in the simulation. For a calcium wave propagation, traveling at a speed of 43 μm/s, it takes around 1.6 s to reach the neighboring well (position 3) for 70 μm channel and around 3.5 s for 150 μm channel. The numbers in bold are the chemical concentrations at the time a calcium wave reaches the position.

the diffusion from the stimulus well to the neighboring wells at 1, 5, and 10 s after stimulus injection.

Table III summarizes the concentration profiles at position 3 at different time points after adding the stimulus for patterns with different channel lengths. The numbers in bold are the concentrations at the time when calcium waves reach position 3. The concentrations were too low to stimulate cell response. However, the concentrations at position 3 in patterns with channel length of 70 μm were higher than that in patterns with a channel length of 150 μm. This indicates the effects of channel length on compound diffusion within microstructures. For chemical depolarization of neural network in MNFSs, channel length should be long enough to distinguish cellular response caused by stimulus from that caused by cell-to-cell communication.

Concentration profiles of the chemical stimulus were studies in situations where tips with larger openings are used for stimulus addition. These results show that the larger the opening, the higher the concentration detected at position 3. More details are presented in Supporting Information (Tables 11S and 2S). In HTS application, tip opening may not be fabricated to as small as 6 μm. For larger tip diameters, channel length can be increased to counteract the effects from wider openings.

CONCLUSION

This study constitutes the first step toward a HTS platform for 3D patterned neural network for application in drug screening as well as in basic research. The results support the following conclusions.

1. Fabricated PLLA scaffolds have nanofibrous structures that mimic collagen fibers in ECM and exhibit higher porosity, improved thermal and mechanical properties than PLLA scaffolds without nanofibrous structures.
2. Laser micromachined patters in the nanofibrous PLLA films are compatible with stem cell culture and integrate easily in high-density-well plates (e.g. 96-well plates) for HTS application.
3. Mathematical simulation confirmed that it is possible to study neural network activity induced by chemical stimulation in these MNFSs and by controlling parameters in MNFSs (such as channel), cellular responses due to cell-to-cell communication can be distinguished from those caused by chemical diffusion.

ACKNOWLEDGMENTS

The authors thank Dr. Bingqian Xu, Dr. Yiping Zhao, Dr. John Shields, Dr. Jianguo Fan, Dr. Ke Cheng, Ms. Yinzhi Lai, Mr. Yanbin Guan and Mr. Roger Hilton for technical assistance.

REFERENCES

1. Javitt DC, Spencer KM, Thaker GK, Winterer G, Hajós M. Neurophysiological biomarkers for drug development in schizophrenia. Nature Rev Drug Discov 2008;7:68–83.
2. Seow D, Gauthier S. Pharmacotherapy of Alzheimer's disease. Can J Psychiatry 2007;52:620–629.
3. Cutler NR, Sramek JJ. Review of the next generation of Alzheimer's disease therapeutics: Challenges for drug development. Prog Neuropsychopharmacol Biol Psychiatry. 2001;25:27–57.
4. Craighead HG, James CD, Turner AMP. Chemical and topographical patterning for directed cell attachment. Curr Opin Solid State Mater Sci 2001;5:177–184.
5. Kane RS, Takayama S, Ostuni E, Ingber DE, Whitesides GM. Patterning proteins and cells using soft lithography. Biomaterials 1999;20:2363–2376.
6. Nicolau DV, Taguchi T, Taniguchi H, Tanigawa H, Yoshikawa S. Patterning neuronal and glia cells on light-assisted functionalized photoresists. Biosens Bioelectron 1999;14:317–325.
7. Vogt AK, Wrobel G, Meyer W, Knoll W, Offenhauser A. Synaptic plasticity in micropatterned neuronal networks. Biomaterials 2005;26:2549–2557.
8. Stevens MM, Mayer M, Anderson DG, Weibel DB, Whitesides GM, Langer R. Direct patterning of mammalian cells onto porous tissue engineering substrates using agarose stamps. Biomaterials 2005;26:7636–7641.
9. Yousaf MN, Houseman BT, Mrksich M. Using electroactive substrates to pattern the attachment of two different cell populations. PNAS 2001;98:5992–5996.
10. Wu Z-Z, Zhao Y-P, Kisaalita WS. A pached Cytodex microbead array for three-dimensional cell-based biosensing. Biosens Bioelectron 2006;22:685–693.
11. Wang L, Wu Z-Z, Xu B, Zhao Y, Kisaalita WS. SU-8 microstructure for quasi-three-dimensional cell-based biosensing. Sens Actuators 2009;140:349–355.
12. Griscom L, Degenaar P, LePioufle B, Tamiya E, Fujita H. Cell placement and neural guidance using a three-dimensional microfluidic array. Jpn J Appl Phys 2001;40:5485–5490.
13. Merz M, Fromherz P. Silicon chip interfaced with a geometrically defined net of snail neurons. Adv Funct Mater 2005;15:739–744.
14. Yang F, Murugan R, Ramakrishna S, Wang X, Ma Y-X, Wang S. Fabrication of nano-structured porous PLLAscaffold intended for nerve tissue engineering. Biomaterials 2004;25:1891–1900.
15. Matthews JA, Wnek GE, Simpson DG, Bowlin GL. Electrospinning of collagen nanofibers. Biomacromolecules 2002;3:232–238.
16. Zhang S, Gelain F, Zhao X. Designer self-assembling peptide nanofiber scaffolds for 3D tissue cell cultures. Semin Cancer Biol 2005;15:413–420.
17. Yim EK, Pang SW, Leong KW. Synthetic nanostructures inducing differentiation of human mesenchymal stem cells into neuronal lineage. Exp Cell Res 2007; 15, 313:1820–1829.
18. Patel S, Kurpinski K, Quigley R, Gao H, Hsiao BS, Poo M-M, Li S. Bioactive nanofibers: Synergistic effects of nanotopography and chemical signaling on cell guidance. Nano Lett 2007;7: 2122–2128.
19. Cukierman E, Pankov R, Stevens DR, Yamada KM. Taking cell-matrix adhesions to the third dimension. Science 2001;294: 1708–1712.
20. Yang F, Murugan R, Wang S, Ramakrishna S. Electrospinning of nano/micro scale poly(L-lactic acid) aligned fibers and their potential in neural tissue engineering. Biomaterials 2005;26:2603–2610.
21. Wang S S-H, and Thompson SH. Local positive feedback by calcium in the propagation of intracellular calcium waves. Biophys J 1995;69:1683–1697.
22. Zhang R, Ma PX. Poly(a-hydroxyl acids)/hydroxyapatite porous composites for bone-tissue engineering. I. Preparation and morphology. J Biomed Mater Res 1999;44:446–455.
23. Axelrod D, Koppel DE, Schlessinger J, Elson E Webb WW. Mobility measurement by analysis of fluorescence photobleaching recovery kinetics. Biophys J 1976;16:1055–1069.
24. Leddy HA, Guilak F. Site-specific molecular diffusion in articular cartilage measured using fluorescence recovery after photobleaching. Ann Biomed Eng 2003;31:753–760.
25. Liu X, Lim JY, Donahue HJ, Dhurjati R, Mastro AM, Vogler EA. Influence of substratum surface chemistry/energy and topography on the human fetal osteoblastic cell line hFOB 1.19: Phenotypic and genotypic responses observed in vitro. Biomaterials 2007;28: 4535–4550.

26. Galambos P, Forster FK. Micro-fluidic diffusion coeffeicent measurement. Presented as proceedings at the μTAS' 98 Workshop, Banff, Canada, October 13–16, 1998.
27. Jaffe LF. On the conservation of fast calcium wave speeds. Cell Calcium 2002;32:217–229.
28. Culbertson CT, Jacobson SC, Ramsey JM. Diffusion coefficient measurements in microfluidic devices. Talanta 2002;56:365–373.
29. Chen VJ, Ma PX. Nano-fibrous poly(l-lactic acid) scaffolds with interconnected spherical macropores. Biomaterials 2004;25: 2065–2073.
30. Engler AJ, Sen S, Sweeney HL, Discher DE. Matrix elasticity directs stem cell lineage specification. Cell 2006;126:677–689.
31. Saha K, Keung AJ, Irwin EF, Li Y, Little L, Schaffer DV, Healy KE. Substrate modulus directs neural stem cell behavior. Biophys J 2008;95:4426–4438.
32. Xu H, Teng C, Yu M. Improvements of thermal property and crystallization behavior of PLLA based multiblock copolymer by forming stereocomplex with PDLA oligomer. Polymer 2006;47:3922–3928.
33. Wang Y-Q, Cai J-Y. Enhanced cell affinity of poly(L-lactic acid) modified by base hydrolysis: Wettability and surface roughness at nanometer scale. Curr Appl Phys 2007;7S:e108–e111.